Influence of selected CO_2 absorption promoters on the characteristics of calcium carbonate particles produced by carbonation of the post-distillation liquid from the Solvay process

Natalia Czaplicka [a,*], Donata Konopacka-Łyskawa [a], Patrycja Lewandowska [a], Marcin Łapiński [b], Rafał Bray [c]

[a] *Department of Process Engineering and Chemical Technology, Faculty of Chemistry, Gdansk University of Technology, Narutowicza 11/12, 80-233 Gdansk, Poland*
[b] *Department of Solid State Physics, Faculty of Applied Physics and Mathematics, Gdansk University of Technology, Narutowicza 11/12, 80-233 Gdansk, Poland*
[c] *Department of Water and Wastewater Technology, Faculty of Civil and Environmental Engineering, Gdansk University of Technology, Narutowicza 11/12, 80-233 Gdansk, Poland*

ARTICLE INFO

ABSTRACT

The aim of this work is to compare the effect of selected process parameters, gas flow rate, CO_2 absorption promoter concentration and its pKa, on the precipitation of $CaCO_3$ by the gas-liquid method using a model post-distillation liquid from the Solvay process. To ensure effective capture of CO_2, the absorption promoters used were ammonia, triethanolamine and triethylamine. The Box-Behnken Design was applied to plan the experiments. The analysis of the influence of selected parameters on the course of the process and the characteristics of the obtained products was performed using the response surface methodology. In the studied range of variables, the type of absorption promoter characterized by its pKa has the most significant impact on the reaction time, polymorphic composition of the obtained $CaCO_3$, particle size and their specific surface area. All precipitated $CaCO_3$ samples were highly agglomerated mixture of vaterite and calcite.

1. Introduction

Calcium carbonate occurs extensively in nature in the form of three anhydrous polymorphs, calcite, aragonite and vaterite [1]. Theoretically, calcite is the most thermodynamically stable crystalline form of $CaCO_3$. The other two polymorphs are metastable and transform into a thermodynamically favored calcite by dissolution and recrystallization [2,3]. The formation of a specific crystalline phase is the result of successive steps of nucleation and crystal growth, and the crystallization pathways are controlled by thermodynamic or kinetic steps [4]. The analysis of the nucleation rate for various polymorphs depending on the temperature shows that the nucleation rate for vaterite is the highest at moderate temperatures up to about 40 °C, while above, the nucleation rate for aragonite is dominant [3]. Therefore, at room temperature, both vaterite and calcite is obtained, while aragonite is most often produced at elevated temperatures [2,5]. The crystalline form determines the particle morphology [6,7], solubility [8,9], refractive index [10], and sorption properties [11]. In addition, important parameters determining the use of calcium carbonate are particle size, specific surface area and porosity [12,13].

$CaCO_3$ is used in various products, e.g. in paper [14], plastics and rubber as a pigment or filler [15,16], in environmental protection [17], in

pharmaceuticals as calcium ions source and pH controller [18] or in cosmetics [19] to improve rheology, physical robustness or visual appearance. Precipitated calcium carbonate (PCC) is one of the most commonly used in specialized purity-defined applications. The required $CaCO_3$ features can be controlled by the selection of process parameters. Apart from the temperature, other important parameters during the precipitation of calcium carbonate are supersaturation, pH, the rate of reagent supply, and the intensity of mixing [20,21]. The choice of the reactor and the type of stirrer also have a significant influence on the course of precipitation and the characteristics of the obtained $CaCO_3$ particles [22,23]. Moreover, when the production of calcium carbonate formation is carried out in the gas-liquid system with the use of gaseous CO_2 as a reactant, the course of precipitation is also determined by the control of the rate of CO_2 absorption [24]. Research conducted by Ding et al. [5] indicate that by changing the reaction conditions such as the process temperature and the concentration of the reagents, the morphology of $CaCO_3$ precipitated in the $CaCl_2$-NH_3-CO_2 system can be controlled without the use of additional substances. Kirboga et al. [25] showed that the duration of the use of ultrasound is one of the variables controlling both the surface area and the particle size of $CaCO_3$ crystals. Ukrainczyk et al. [24] investigated the influence of temperature, conductivity, CO_2 flow rate, stirring rate and calcium ion concentration on the reaction efficiency and the specific surface area of the obtained calcium carbonate. According to this research, conductivity and temperature significantly influence particles morphology,

* Corresponding author.
  E-mail address: natalia.czaplicka@pg.edu.pl (N. Czaplicka).

while stirring rate, conductivity and gas flow rate strongly affect the precipitation efficiency [24]. The reaction with gaseous carbon dioxide is specific, because the formation of bicarbonate ions during CO_2 absorption with chemical reaction is a limiting step of the $CaCO_3$ precipitation process [26]. The yield of calcium carbonate precipitation in a gas-liquid system depends on the ratio of concentration of Ca^{2+}/promoter [27], the volume fraction of carbon dioxide in the gas stream supplied to the reactor [28,29] and the type of absorption promoters [30,31]. Investigated CO_2 absorption promoters have been: ammonia [32], and selected amines like mono-, and triethanolamine [30], mono-, di- and triethylamine [26].

Recently, there are many studies in the literature on the use of calcium-rich waste as substrates for the production of calcium carbonate [33,34]. The use of the gas-liquid method for this purpose allows both the disposal of problematic industrial waste and the sequestration of CO_2 from exhaust gases. One of the processes in which generated waste can be a source of Ca^{2+} in the $CaCO_3$ precipitation, is the Solvay process [35,36]. The produced post-distillation liquid contains mainly calcium chloride with a concentration of 1.010 mol/L [33]. In soda plants using the Solvay method, the waste post-distillation liquid is mainly stored in landfills called white seas. This leads to the salinity of the surrounding soil and groundwater, which is a serious environmental threat [35]. Therefore, finding alternative methods for the management of this type of waste is an important environmental issue.

The aim of this study was to compare the effect of selected process parameters on the precipitation of calcium carbonate by the gas-liquid method using a model post-distillation liquid from the Solvay process. Based on previous experiments, the parameters tested were the type of absorption promoter, its concentration and gas flow rate. The Box-Behnken Design (BBD) was used to plan the experiments. The analysis of the influence of selected parameters on the course of the process and the characteristics of the obtained products was performed using the response surface methodology (RSM).

2. Materials and methods

2.1. Materials

Anhydrous calcium chloride (POCH, Poland), sodium chloride (P.P.H. STANLAB, Poland), 25% ammonia solution (POCH, Poland), triethanolamine (TEA) (Chempur, Poland), triethylamine (Et_3N) (Chempur, Poland), methanol (POCH, Poland), di-sodium wersenate, standard solution 0.1 mol/L (Chempur, Poland), buffer solution pH 10 ± 0.05 (Chempur, Poland), eriochrome black T (Chempur, Poland). All reagents were of analytical grade and were used without further purification. The water obtained by reverse osmosis was used to prepare all solutions.

2.2. Particles preparation

Calcium carbonate particles were precipitated at atmospheric pressure (1013 hPa) and room temperature (22 °C) using carbonation method in passive CO_2 capture system. Model post-distillation liquid from the Solvay process with a volume of 0.2 L was used as a reaction mixture. Such aqueous solution contained 1.01 mol/L of calcium chloride and 0.966 mol/L of sodium chloride. Precipitation reaction was carried out in an open glass tank reactor with a total volume of 0.3 L. The reaction mixture was stirred at 700 rpm using a magnetic stirrer. The scheme of the experimental set up is presented in our previous work [37]. Three absorption promoters with different pKa values were used: TEA (pKa = 7.79), ammonia (pKa = 9.25) and Et_3N (pKa = 10.81), and were added to the reaction mixture in various molar ratios with respect to calcium ions ([promoter]:[Ca^{2+}] = 1.5:1, 2:1 and 2.5:1). The promoter concentrations were 1.515, 2.020 and 2.525 mol/L, respectively. Gaseous CO_2 in a mixture with air ($x_{v,CO2}$ = 0.15) was continuously supplied into the liquid phase through a porous glass plate and

gas mixing occurred during the flow, before it was supplied into the reaction mixture. The gas mixture flow rate was 60, 70 and 80 L/h. The course of the reaction was monitored by measuring the pH of the reaction solution using composite electrode (ERH — 111 type, HYDROMET, Poland) connected to the computer. The precipitation process was carried out until the pH was reached 7. Complexometric titration of collected samples (0.002 L) with EDTA was used to determine the initial and final Ca^{2+} concentration. Obtained $CaCO_3$ powder was filtered and washed with water and methanol, and dried for 24 h at 90 °C.

2.3. Particles characterization

To characterize polymorphic composition and crystalline structure of precipitated $CaCO_3$ conventional powder X-ray diffraction technique (XRD) with Cu-Kα radiation was applied using the MiniFlex 600 diffractometer (Rigaku, Tokyo, Japan). The XRD analysis was carried out at room temperature, at 0.2º scan rate and 2θ angle range of 20-80º. Additionally, Fourier transform infrared spectroscopy (FT-IR) was applied using the Nicolet 8700 Spectrometer (Thermo Scientific, Waltham, MA, USA). The suppressed total reflection (ATR) method was used. Spectra were registered from 4000 to 500 cm^{-1} at 2 cm^{-1} resolution using air as the background. Specific surface area and pore size of obtained calcium carbonate particles were determine using the Brunauer-Emmett-Teller (BET) method. These parameters were evaluated from the adsorption-desorption isotherms of liquid nitrogen (77 K) detected using Surface Area Analyzer Gemini V (model 2365, Micromeritics, Norcross, GA, USA). Before measuring, 0.1 g of the sample was dried and degassed for 2 h at 200 °C. The size of precipitated particles was determined by a laser diffraction method using the analyzer Mastersizer 2000 (Malvern Panalytical Ltd., Malvern, United Kingdom) equipped with a standard dispersion units Hydro 2000MU with an ultrasonic probe supporting the breaking of agglomerates. The range of particle diameter measurement was between 0.02 and 2000 µm. FEI Quanta FEG 250 scanning electron microscope (SEM) equipped

Table 1
Range and levels of parameters in Box-Behnken experimental design.

Factors	Parameters	Coded levels		
		−1	0	1
A	Promoter concentration [mol/dm³]	1.515	2.020	2.525
B	Gas flow rate [dm³/h]	60	70	80
C	pKa of the promoter	7.8	9.3	10.8

Table 2
Box-Behnken matrix.

Experiment number	A	B	C	Promoter concentration [mol/dm³]	Gas flow rate [dm³/h]	pKa of the promoter
1	−1	−1	0	1.515	60	9.3
2	+1	−1	0	2.525	60	9.3
3	−1	+1	0	1.515	80	9.3
4	+1	+1	0	2.525	80	9.3
5	−1	0	−1	1.515	70	7.8
6	+1	0	−1	2.525	70	7.8
7	−1	0	+1	1.515	70	10.8
8	+1	0	+1	2.525	70	10.8
9	0	−1	−1	2.020	60	7.8
10	0	+1	−1	2.020	80	7.8
11	0	−1	+1	2.020	60	10.8
12	0	+1	+1	2.020	80	10.8
13	0	0	0	2.020	70	9.3
14	0	0	0	2.020	70	9.3
15	0	0	0	2.020	70	9.3

Table 3
Box-Behnken results: percentage consumption of calcium ions (%Ca^{2+}), percentage vaterite content (X_V), specific surface area (BET), pore volume (V_{por}), and median size (d_{50}) of $CaCO_3$ particles.

Experiment number	Response					
	t_r [min] y_1	%Ca^{2+} [%] y_2	X_V [%] y_3	d_{50} [μm] y_4	BET [m^2/g] y_5	V_{por} [cm^3/g] y_6
1	73	54.7	10.79	11.4	1.1626	0.0015
2	76,5	84.7	33.83	14.0	1.5482	0.0019
3	58	56.2	9.45	12.1	0.9358	0.0013
4	65,5	83.7	18.31	11.6	0.8441	0.0012
5	78	54.2	80.62	9.5	1.5418	0.0019
6	111	69.1	83.52	9.4	1.1393	0.0013
7	52	43.8	9.51	6.6	3.9683	0.0054
8	91	77.7	8.38	9.0	4.0551	0.0058
9	110	59.5	89.62	11.0	0.7674	0.0011
10	114	62.6	78.30	12.7	1.1511	0.0013
11	46,5	63.6	7.85	5.7	2.5212	0.0038
12	64	47.5	11.05	4.9	3.4915	0.0044
13	100,5	62.9	67.80	14.8	1.1325	0.0014
14	112	68.8	68.40	14.8	1.1542	0.0014
15	110	65.5	67.50	14.7	1.1289	0.0014

with an Everhart-Thornley (ET) secondary electron detector (FEI, Hillsboro, OR, USA) was applied to characterize the shape of obtained $CaCO_3$ particles.

2.4. Experimental design

To determine the effect of selected variables on the efficiency of the precipitation process, the percentage content of vaterite in the obtained samples, the specific surface area, the pore volume and the median diameter of precipitated $CaCO_3$ particles, the response surface methodology (RSM) as a statistical method was applied. Using the Minitab 19 Statistical Software (Minitab Inc., State College, PA, USA), an experiment design was constructed exploit a three-level-three-factor Box-Behnken plan. As the independent variables, promoter concentration (A), gas flow rate (B) and pKa of the promoter (C) were chosen. Each of the parameters was tested on three levels: low (-1), high ($+1$) and midpoint (0). The values of levels for individual variables are summarized in Table 1.

The use of the Box-Behnken design method allows adjustment of the quadratic surface and creation of the second-order polynomial model presented by Eq. (1). Moreover, thanks to this method, it is possible to analyze the interactions between the independent variables with the minimum number of experiments. The total number of experiments required is 15 and a matrix showing the parameters of each run is summarized in Table 2.

$$y = \beta_0 + \sum_{i=1}^{n} \beta_i x_i + \sum_{i=1}^{n} \beta_{ii} x_i^2 + \sum_{i=1}^{n} \sum_{j>1}^{n} \beta_{ij} x_i x_j \qquad (1)$$
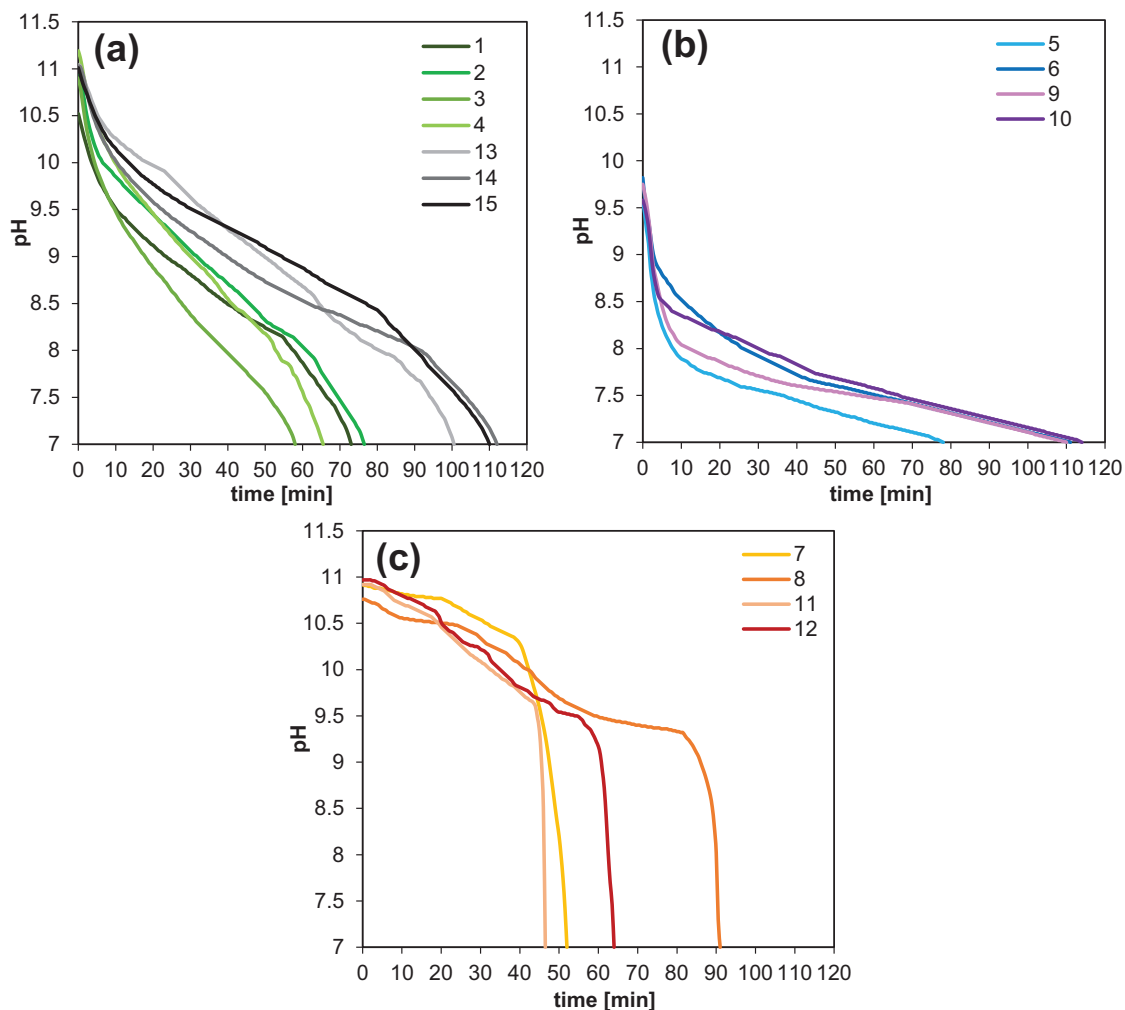

Fig. 1. pH versus reaction time curves for all experiments depending on CO_2 absorption promoter: (a) ammonia, (b) TEA, (c) Et$_3$N.
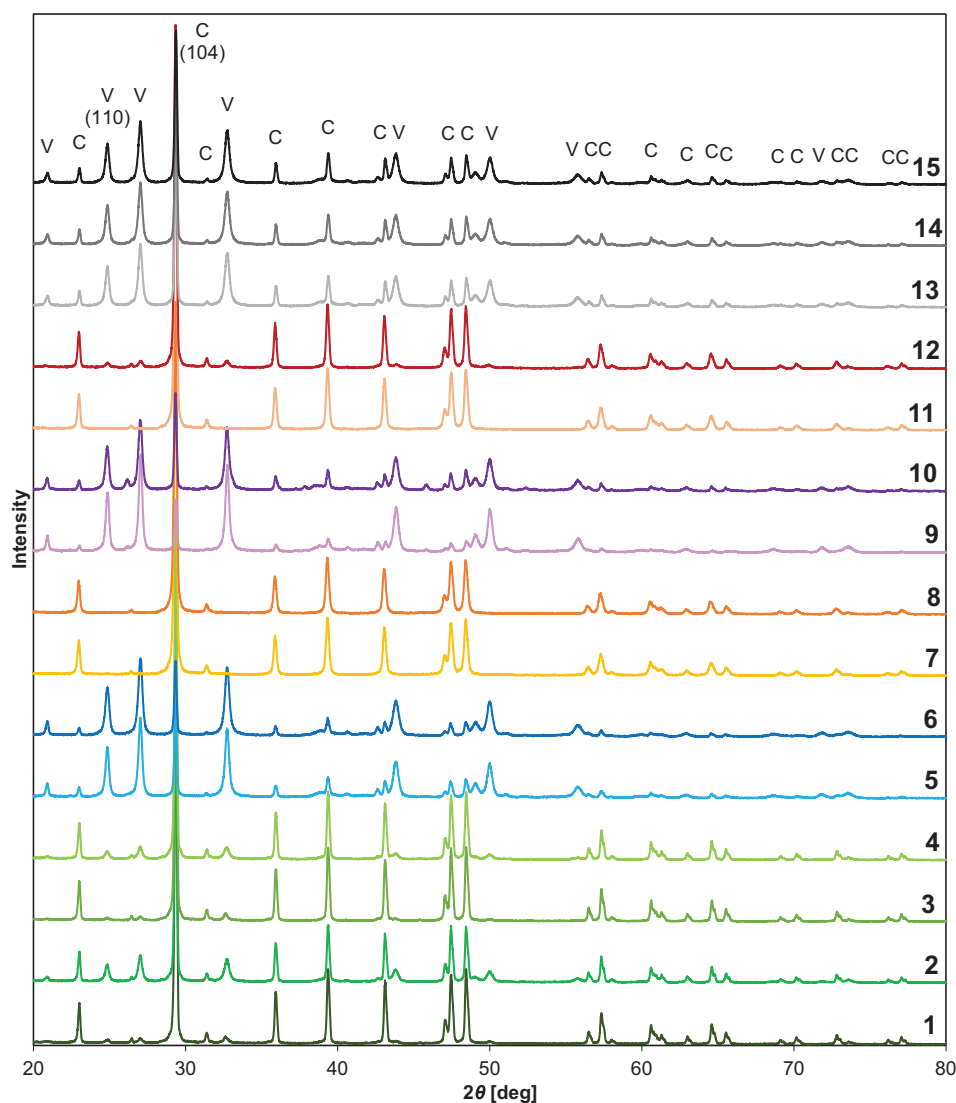
Fig. 2. XRD patterns of calcium carbonate obtained in all experiments.

where x – independent variable, y – predicted response, β_0 – constant term, β_i – linear coefficient, β_{ii} – quadratic coefficient, β_{ij} – interaction coefficient.

3. Results and discussion

3.1. Experimental design results

Table 3 summarizes the results obtained from all 15 experiments planned with BBD. The responses are the reaction time (t_r), the percentage of calcium ion consumption ($\%Ca^{2+}$), the percentage of vaterite in the precipitated calcium carbonate (X_v), the specific surface area (BET) and pore volume (V_{por}) of the obtained particles and their median size (d_{50}). Based on results from Table 3, polynomial equations in uncoded units presenting the empirical relationship between the responses and selected independent variables were determined and presented in subsequent chapters of this work. Furthermore, 3D response surfaces as a function of two variables maintaining all parameters at fixed levels were prepared. It is a graphic representation of the designated polynomial equation. By analyzing these graphs, it was determined whether the relationship between the responses and individual independent variables is linear or quadratic. Based on BBD, an ANOVA was also

performed and Pareto charts were made for all responses, which enabled the effects of which variables and interactions are statistically significant to be indicated. A high F-value and p-value less than or equal to the significance level ($\alpha = 0.05$) indicate that the model is statistically significant.

3.2. The course of the precipitation process

Due to the reactions of bicarbonate and carbonate ions formation occurring during the carbonation process, the pH of the reaction mixture is decreased. Therefore, measuring changes in the pH of the solution allows monitoring of the precipitation rate. Graphs of pH versus reaction time for all experiments grouped according to the CO_2 absorption promoter are shown in Fig. 1. Each of the absorption promoter is characterized by a specific course of the pH changes as a function of time.

3D response surfaces for the reaction time as a function of two variables are shown in Supplementary Materials in Fig. S1. Polynomial equation presenting the empirical relationship between the reaction time (y_{tr}) and selected independent variables is given by Eq. (2). The value of the coefficient of determination (R^2) for this model equals 0.83. ANOVA analysis (Supplementary Materials, Table S1) and obtained Pareto chart (Supplementary Materials, Fig. S2) show that the
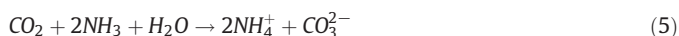
type of absorption promoter (C) has the greatest impact on the reaction time. Only for this variable, the p-value is lower than the significance level ($p \leq \alpha$) and the exceeding of the baseline (2.571) in the Pareto chart is observed, which indicates that effect of promoter pKa is statistically significant. The response surfaces graphs also show that the relationship between the reaction time and the type of promoter in the studied range is linear. The higher the promoter pKa, the shorter the reaction time. The longest precipitation reaction was carried out with the use of TEA (pKa 7.8) with a concentration of 2.020 mol/L and when the gas mixture flow was set at its highest applied rate of 80 L/h. The shortest precipitation time was observed at the same gas flow rate and concentration of the promoter, which was Et_3N (pKa 10.8).

$$y_{t_r} = -1035 + 304A + 24.5B + 4.7C - 78.2A^2 - 0.1931B^2 - 2.03C^2 + 0.2AB + 2AC + 0.225BC \tag{2}$$

Graphs showing 3D response surfaces for the consumption of calcium ions as a function of two variables (Supplementary Materials, Fig. S3) were made. The designated polynomial equation presenting the empirical relationship between the calcium ions consumption ($y_{\%Ca2+}$) and selected independent variables is described by Eq. (3). The value of the coefficient of determination (R^2) for this model equals 0.97. It turns out that the greatest influence on the consumption of Ca^{2+} ions is the concentration of the CO_2 absorption promoter (A). This is confirmed by the ANOVA results (Supplementary Materials, Table S2) and the Pareto chart (Supplementary Materials, Fig. S4) obtained on the basis of BBD. For the promoter concentration, promoter pKa, interaction between pKa and gas flow rate, and interaction between pKa and promoter concentration, the p-value is lower than the significance level ($p \leq \alpha$) and the exceeding of the baseline (2.571) in the Pareto chart is observed, which on the one hand indicates that the effect of these variables is statistically significant. On the other hand, 3D response surfaces indicate that the consumption of calcium ions increases with increasing promoter concentration and in the studied range this relationship is linear. In the case of the promoter pKa (C), the relationship is square with the maximum at the value of 9.3, i.e. for ammonia. Therefore, the highest values of the consumption of Ca^{2+} ions were obtained in the case of the reaction using ammonia (pKa 9.3) with the highest tested concentration (2.525 mol/L). They are respectively 84.7% and 83.7% for gas flow rates 60 and 80 L/h. Thus, the slight difference in the obtained values indicates a slight influence of the gas flow rate on this response.

$$y_{\%Ca^{2+}} = -298 - 78.7A + 2.24B + 75C + 13.71A^2 + 0.006B^2 - 3.569C^2 - 0.124AB + 6.27AC - 0.32BC \tag{3}$$

In ammonia solutions, the maximum theoretical ratio $CO_2:NH_3$ depends on the conditions of reaction and $CO_2:NH_3$ is equal 1:2 when carbonate or carbamate ions are formed, while the ratio $CO_2:NH_3$ is 1:1 when bicarbonate ions are produced during CO_2 absorption. The formation of carbamate, bicarbonate and carbonate ions in the case of ammonia is described by Eqs. (4)–(6).

$$CO_2 + 2NH_3 \rightarrow NH_2COO^- + NH_4^+ \tag{4}$$

$$CO_2 + 2NH_3 + H_2O \rightarrow 2NH_4^+ + CO_3^{2-} \tag{5}$$

$$NH_2COO^- + H_2O \rightarrow NH_3 + HCO_3^- \tag{6}$$

In triethanolamine and triethylamine solutions, the maximum theoretical CO_2 loading is 1:1 due to the base-catalyzed hydration mechanism of carbon dioxide absorption [30] described by Eq. (7).

$$CO_2 + R_3N + H_2O \rightarrow HCO_3^- + R_3N^+ \tag{7}$$
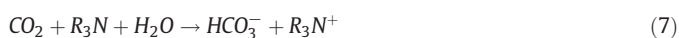
Previous studies have also indicated an impact of the ratio of concentration of $CaCl_2$/promoter [27], the volume fraction of carbon dioxide in the gas stream supplied to the reactor [28,29], and the type of absorption promoters [30,31] on the yield of calcium carbonate precipitation in a gas-liquid system. The method used in this study showed that in the studied range of variables, the selection of the absorption promoter and its concentration have a significant impact on both the degree of Ca ions conversion and the reaction time.

3.3. Percentage vaterite content

In all the experiments, the obtained samples of calcium carbonate were a mixture of two polymorphs, vaterite and calcite, which is confirmed by the XRD diffractograms presented in Fig. 2, and FTIR-ATR spectra (Supplementary Materials, Fig. S5). Polymorph composition of $CaCO_3$ samples was determined on the basis of XRD patterns. The Eq. (8) proposed by Kontoyannis and Vagenas was used to calculated the vaterite fraction in precipitates [38].
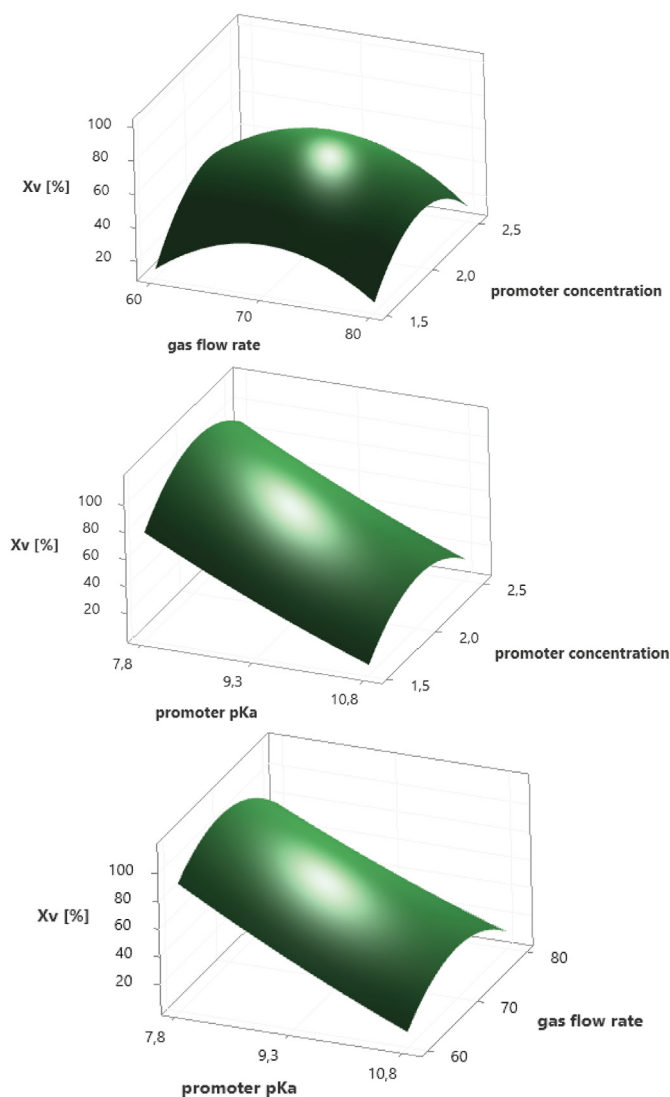

Fig. 3. 3D surface plots presenting the effect of (a) promoter concentration and gas flow rate, (b) promoter concentration and promoter pKa, and (c) gas flow rate and promoter pKa on percentage vaterite content in obtained $CaCO_3$.

$$X_V = \frac{7.691 I_V^{110}}{I_C^{104} + 7.691 I_V^{110}} \qquad (8)$$

where X_V is the fraction of vaterite in the calcite-vaterite mixture, I_V is the intensity of the reflection peak at (110) for vaterite and I_C at (104) for calcite. The percentage vaterite contents in the samples are summarized in Table 3.

Polynomial equation obtained in uncoded units presenting the empirical relationship between the percentage vaterite content and selected independent variables is described by Eq. (9). The R^2 value for this model equals 0.99, which indicates strong agreement between the experimental and predicted responses. According to ANOVA (Supplementary Materials, Table S3), the p-value is lower than the significance level ($p \leq \alpha$) and the exceeding of the baseline (2.571) in the Pareto chart (Supplementary Materials, Fig. S6) is observed for promoter concentration (A^2), gas flow rate (B^2) and promoter pKa (C). The p-value for the model described by Eq. (9) is 0, which indicates significant model fit. Additionally, analyzing the 3D response surfaces shown in Fig. 3, it can be concluded that in the studied range of variables, the influence of promoter pKa on the vaterite content is linear, while in the case of gas flow rate and promoter concentrations, the relationships are quadratic. According to the model, the samples obtained in the reaction with TEA (lowest pKa) at concentration of 2.020 mol/L (average value) with a gas flow of 70 L/h (average value) should be characterized by the highest content of vaterite.

$$y_{X_V} = -1144 + 473.8A + 32.88B - 64.6C - 100A^2 - 0.243B^2$$
$$+ 1.38C^2 - 0.702AB - 1.33AC + 0.242BC \qquad (9)$$

The study of the mechanism of calcium carbonate formation led to the distinction of the following stages of crystallization carried out at room temperature: (i) formation of amorphous calcium carbonate, (ii) transformation of amorphous calcium carbonate to thermodynamically unstable vaterite, and (iii) slow recrystallization of vaterite into thermodynamically stable calcite. Vaterite formation is kinetically privileged and depends primarily on temperature and supersaturation [2,5,39]. Moreover, when the reaction is carried out at room temperature and basic pH, the dominant crystal form in the product is vaterite [21,32,39,40], and the proportion of vaterite decreases when the pH of the reaction mixture is greater than 9. However, its content in the product is also determined by the rate of transformation of the metastable form into calcite, which can be inhibited, for example, by the presence of inorganic and organic additives [1,37] or carbamate ions formed in ammonia solutions (Eq. (4)) [26,41]. During precipitation with carbon dioxide gas, the CO_2 absorption is an important step, which allows for the generation of supersaturation in the system. High pH promotes CO_2 absorption, and the addition of absorption promoters with pKa above 7 increases the initial pH values of the reaction mixtures. Moreover, in alkaline solutions, CO_2 forms with water the carbonates and bicarbonates necessary for the precipitation reaction. For the absorption promoters used in these studies, the rate of CO_2 transport from the gas phase to the liquid phase increases in the TEA, Et_3N and NH_3 series [42,43]. In previous studies, a mixture of vaterite and calcite was prepared in the presence of ammonia and monoethanolamine, when the time for passing CO_2 through a 0.2 mol/L $CaCl_2$ solution was relatively long and set at 60 min. However, the currently planned tests, when the $CaCl_2$ solution was used with a concentration of 1.01 mol/L, and NaCl was a component of the reaction mixture, the precipitation time
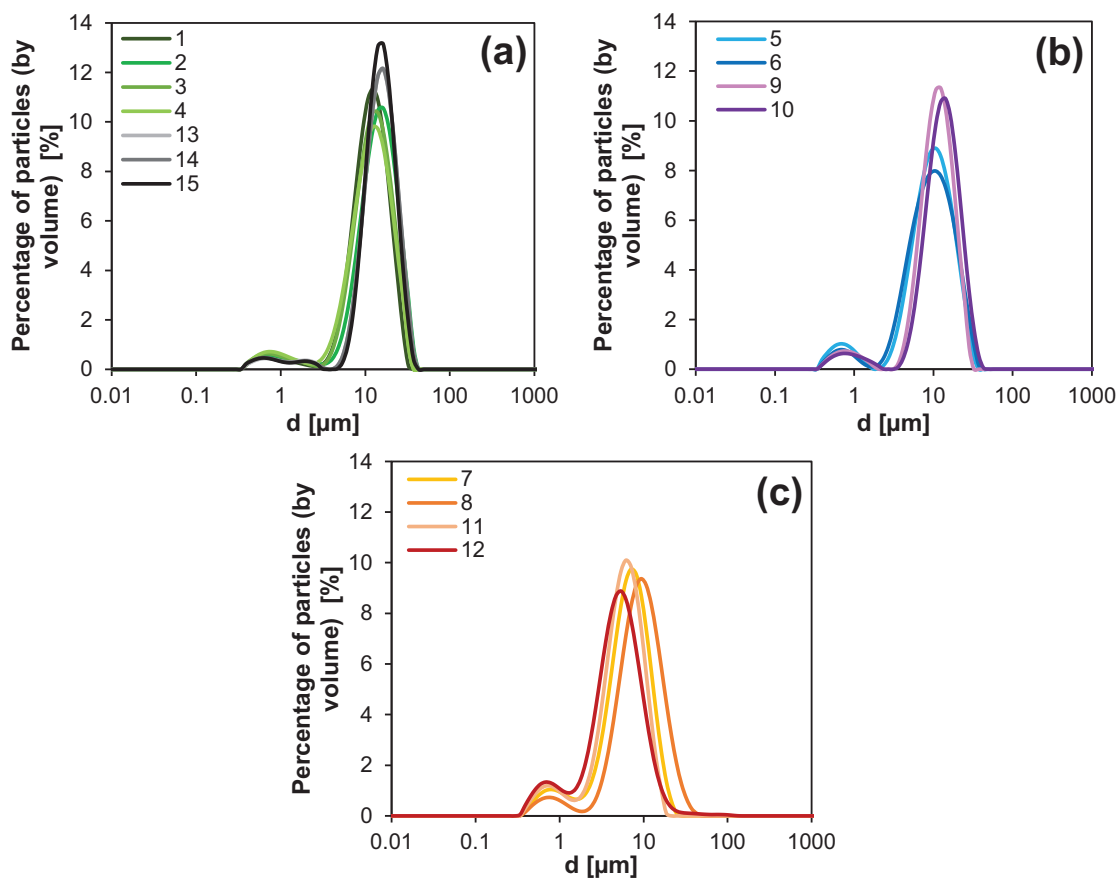

Fig. 4. Particles size distributions (PSDs) depending on absorption promoter: (a) NH_3, (b) TEA, (c) Et_3N.

was relatively shorter and resulted from reaching the pH = 7. Therefore, the highest content of vaterite was obtained in calcium carbonate obtained in the presence of TEA, when the pH of the solution during the reaction was in the optimal range for obtaining vaterite (Fig. 1b). In contrast, the lowest content of vaterite was when Et_3N was the absorption promoter. Then the precipitation took place at high pH, with a moderate rate of absorption, which made it possible to recrystallize the vaterite particles formed at the beginning of the reaction. On the other hand, in the case of the addition of ammonia, the absorption of CO_2 is the fastest and vaterite recrystallization is also possible, but the presence of carbamate ions may inhibit this process.

3.4. Particle size

The calcium carbonate volume-based median particle diameter, d_{50}, of a log-normal distribution was measured after the treatment with ultrasound because the particles stick together during drying. Particle size distributions (PSDs) of all collected samples depending on CO_2 absorption promoter are included in Fig. 4. All the particle size distributions had a similar log-normal course. However, in all cases, presence of a small particle fraction with a maximum of about 700 nm can be also noticed, which indicates the presence of so-called primary crystals in the samples.

Based on the obtained median particle size values, 3D surface plots were prepared and presented in Fig. 5 and polynomial equation describing the empirical relationship between the median particle size (y_{d50}) and independent variables is given by Eq. (10).

$$y_{d_{50}} = -279.7 + 23.5A + 2.48B + 40.78C - 4.82A^2 - 0.01272B^2 \\ -2.198C^2 - 0.155AB + 0.85AC + 0.0426BC \tag{10}$$

The R^2 value of this model is 0.91. According to ANOVA (Supplementary Materials, Table S4) and Pareto chart (Supplementary Materials, Fig. S7) it can be determined, that only promoter pKa has a significant effect on median $CaCO_3$ particle size. Moreover, this relationship is square with a maximum value of 9.3 (ammonia). Thus, the largest particles were obtained with the use of ammonia, and the smallest with the use of Et_3N. The remaining variables, i.e. promoter concentration and gas flow rate, show a slight influence on the particle size, although it can be noticed that the largest particles were precipitated in the reactions using the average values of these parameters, i.e. 2.020 mol/L and 70 L/h.

The size of the particles that are formed in the precipitation process depends on nucleation, crystal growth and agglomeration. According to the classical theory of nucleation, the critical size of a stable nucleus (r_{cr}) can be calculated from the relationship described by Eq. (11).

$$r_{cr} = \frac{2\sigma}{kT\ln S} \tag{11}$$

where σ is the specific surface energy, S is the supersaturation, k is the Boltzmann constant and T is the temperature. This relationship shows that the greater the supersaturation in the solution, the smaller the stable nucleus can be formed. The activity-based supersaturation is defined by Eq. (12).

$$S_a = \left(\frac{a_{Ca^{2+}} a_{CO_3^{2-}}}{K_{sp}}\right)^{1/2} \tag{12}$$

where K_{sp} is the solubility product. The concentration of carbonate ions in the reaction mixture depends on the pH of the solution, which is affected by the dissociation of the absorption promoter added. A solution containing a substance with a higher dissociation constant (pKa) will have a higher concentration of OH- ions (higher pH value). Therefore, when the pH of the solution is higher, as in the case of Et_3N solutions, the concentration of carbonate ions is higher, which allows to produce
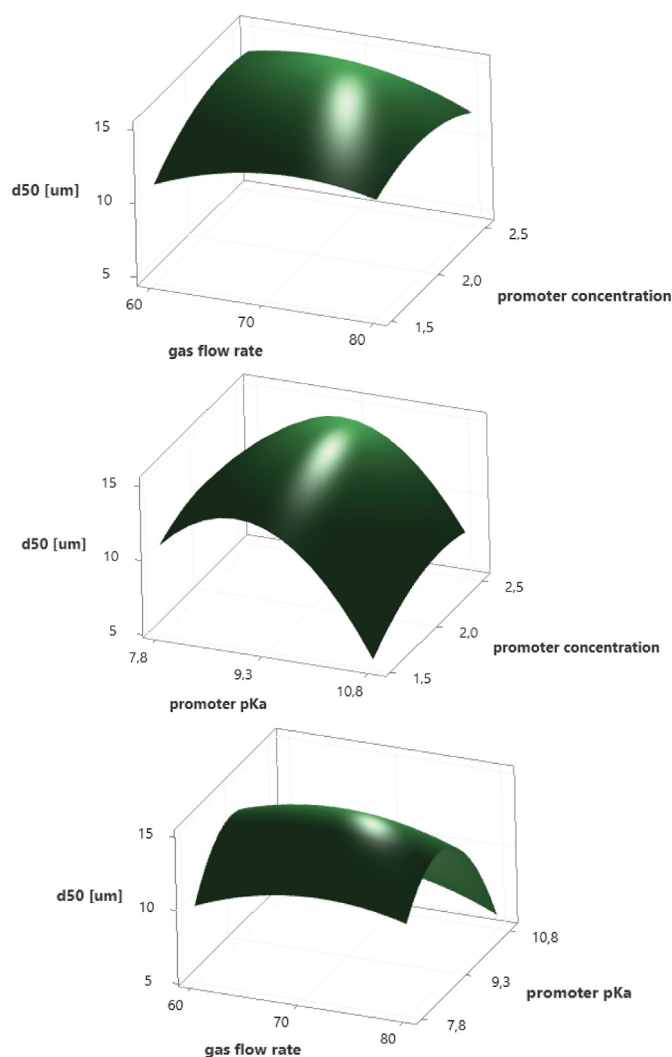

Fig. 5. 3D surface plots presenting the effect of (a) promoter concentration and gas flow rate, (b) promoter concentration and promoter pKa, and (c) gas flow rate and promoter pKa on median particle size of obtained $CaCO_3$.

a higher supersaturation in the solution and hence a smaller size of nuclei and a greater number of them.

In all experiments, the particles obtained were in the form of agglomerates, and the largest agglomerates consisting of deformed calcite particles were obtained in ammonia solutions. Comparing the size of the $CaCO_3$ particles obtained in this experiment when the $CaCl_2$ concentration was 1.01 mol/L in the presence of sodium chloride to the calcium carbonate particles obtained from a solution with a concentration of 0.2 mol/L $CaCl_2$ [30], a similar effect of the absorption promoter can be noticed, i.e. in both experiments the size of the particles obtained in the presence of ammonia is the largest, and in the presence of Et_3N the smallest.

3.5. Specific surface area

The polynomial equation representing the empirical relationship between the specific surface area (y_{BET}) and selected independent variables is given by Eq. (13). The R^2 value equals 0.95, which indicates that this model is statistically significant. Furthermore, the p-value is equal 0.008, so it is lower than α. Thus, there is only 0.8% chance that such a large F-value could occur due to noise. ANOVA results (Supplementary Materials, Table S5) and Pareto chart (Supplementary
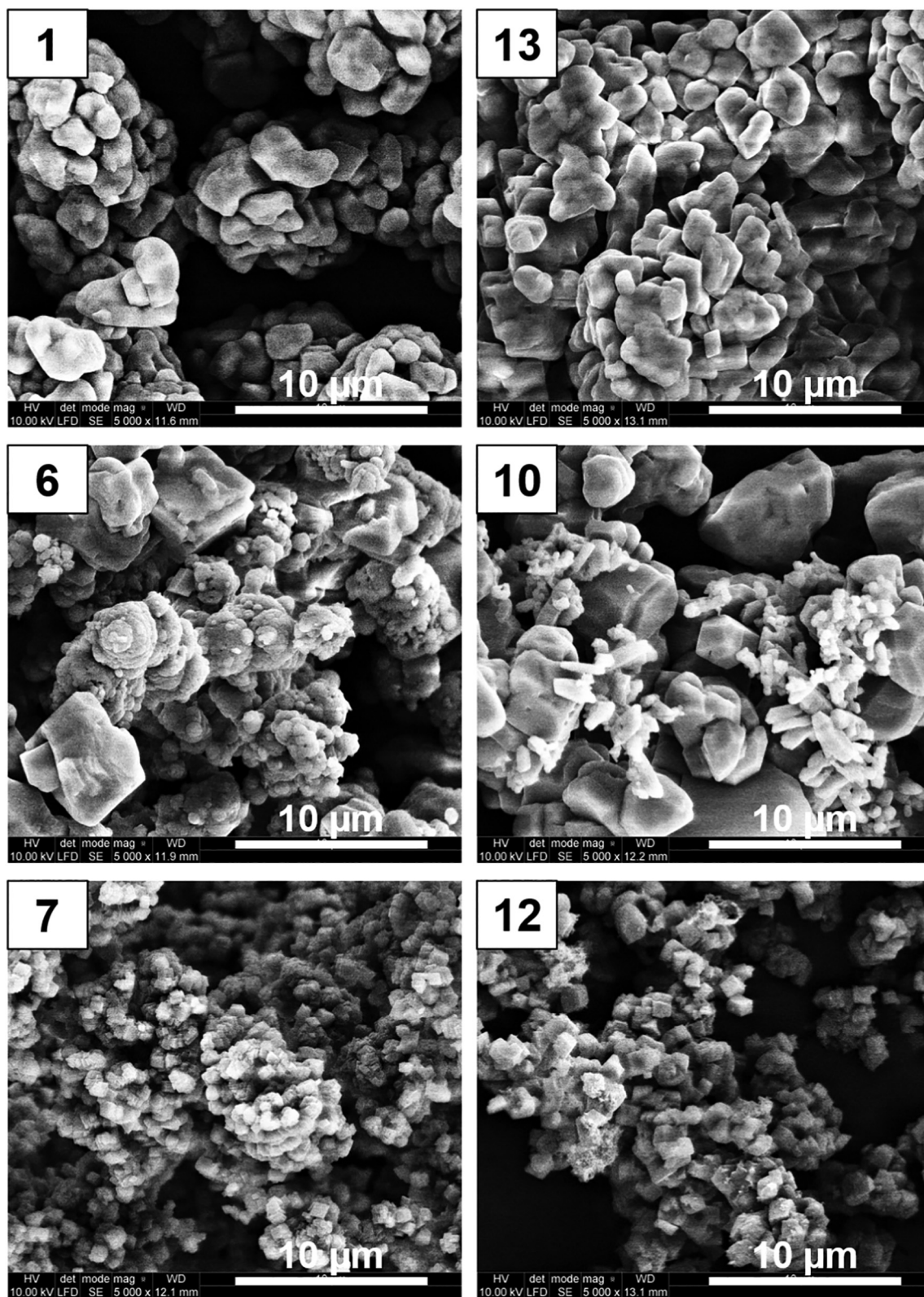
Fig. 6. SEM photographs of selected samples (5000× magnification): 1 – NH_3, 1.515 mol/dm^3, 60 dm^3/h, 6 – TEA, 2.525 mol/dm^3, 70 dm^3/h, 7 – Et_3N, 1.515 mol/dm^3, 70 dm^3/h, 10 – TEA, 2.020 mol/dm^3, 80 dm^3/h, 12 – Et_3N, 2.020 mol/dm^3, 80 dm^3/h, 13 – NH_3, 2.020 mol/dm^3, 70 dm^3/h.

Materials, Fig. S8) demonstrate that only the promoter pKa (C) shows statistical significance. Surface plots (Supplementary Materials, Fig. S9) also indicate, that promoter concentration (A) and gas flow rate (B) have no important influence on specific surface area of

precipitated particles. The samples obtained during the reaction with Et_3N (the highest pKa) have the highest BET values. Due to the fact that the surface pore volume is directly proportional to the specific surface area, analogous relationships for both parameters are observed. The

polynomial equation for surface pore volume ($y_{V_{por}}$) is presented by Eq. (14). R^2 value for this model equals 0.97, which indicates statistical significance.

$$y_{BET} = 33.7 - 5.22A + 0.459B - 10.13C + 1.328A^2 - 0.00355B^2 + 0.5328C^2 - 0.0236AB + 0.161AC + 0.0098BC \quad (13)$$

$$y_{V_{por}} = 0.0494 - 0.00943A + 0.000599B - 0.01393C + 0.00201A^2 - 0.000004B^2 + 0.00075C^2 - 0.000025AB + 0.00033AC + 0.000007BC \quad (14)$$

The specific surface area of the obtained calcium carbonate particles with a small surface pore volume (Table 3) is inversely proportional to the d_{32} particle size. The highest values of specific surface area were obtained in the Et$_3$N solution when particles with the smallest median diameter were precipitated. The theoretically calculated specific surface area for experiments No. 7, 8, 11 and 12 is 0.601, 0.643, 0.685 and 0.785 m^2/g, respectively, and is smaller than that determined on the basis of BET adsorption isotherms. The specific surface areas determined by the N$_2$ adsorption method and calculated from the particle size distribution are of similar values when the particles are perfectly spherical and non-porous. However, the calcium carbonate particles produced in this work are irregular agglomerates. The CaCO$_3$ synthesized in the presence of Et$_3$N have primary crystals about 500 nm in size, as seen in the SEM images (Fig. 6).

3.6. Particle morphology

Morphology of calcium carbonate particles was characterized based on SEM photographs. Pictures of selected samples obtained at a magnification of 5000× depending on the type of absorption promoter are presented in Fig. 6. The particles precipitated during all processes were agglomerated. Samples that were precipitated in the presence of ammonia are characterized by deformed particles with a smooth surface and unsharp edges. Deformed rhombohedral calcite particles can be observed as well as deformed spherical vaterite particles. In the case of TEA, the resulting particles consist mainly of vaterite with a porous surface and lenticular and spherical shape. Smooth rhombohedral and slightly deformed calcite particles are also visible. The use of Et$_3$N results in obtaining particles much finer than in the case of the other absorption promoters used. Smooth rhombohedral calcite particles with sharp edges are also visible.

4. Conclusions

The production of precipitated calcium carbonate from the post-distillation waste solution generated in the Solvay technology is an interesting approach to waste management. In addition, the use of gaseous CO$_2$, which may come from fuel combustion, is also in line with the current trends in research on carbon capture, sequestration and utilization technologies. In this study, the influence of selected process parameters, i.e. pKa and concentration of the absorption promoter as well as the gas flow rate, on the calcium carbonate precipitation process from a model post-distillation solution containing CaCl$_2$ and NaCl was demonstrated. To ensure effective capture of CO$_2$, the following absorption promoters were added: ammonia, triethanolamine and triethylamine differing in pKa values. The use of the Box-Behnken Design method of planning experiments combined with the response surface methodology allowed to state that in the studied range of variables, the type of absorption promoter characterized by its pKa has the most significant impact on the reaction time, polymorphic composition of the obtained calcium carbonate, particle size and their specific surface area. However, the concentration of the absorption promoter significantly affects the consumption of calcium ions. All CaCO$_3$ particles produced were agglomerates and consisted of a mixture of vaterite and calcite. The highest content of vaterite was obtained in experiments with TEA, and the lowest in Et$_3$N solutions. The calcium carbonate particles with the largest median diameter were formed in the presence of ammonia, while the CaCO$_3$ particles produced in the Et$_3$N solution had the largest specific surface area.

Declaration of Competing Interest

The authors declare that they have no known competing financial interests or personal relationships that could have appeared to influence the work reported in this paper.

Appendix A. Supplementary data

Supplementary data to this article can be found online at https://doi.org/10.1016/j.powtec.2021.06.042.

References

[1] D.B. Trushina, T.V. Bukreeva, M.N. Antipina, Size-controlled synthesis of Vaterite calcium carbonate by the mixing method: aiming for nanosized particles, Cryst. Growth Des. 16 (2016) 1311–1319, https://doi.org/10.1021/acs.cgd.5b01422.

[2] J. Chen, L. Xiang, Controllable synthesis of calcium carbonate polymorphs at different temperatures, Powder Technol. 189 (2010) 64–69, https://doi.org/10.1016/j.powtec.2008.06.004.

[3] D. Zhao, Y. Zhu, F. Li, Q. Ruan, S. Zhang, L. Zhang, F. Xu, Polymorph selection and nanocrystallite rearrangement of calcium carbonate in carboxymethyl chitosan aqueous solution: thermodynamic and kinetic analysis, Mater. Res. Bull. 45 (2010) 80–87, https://doi.org/10.1016/j.materresbull.2009.08.015.

[4] H. Cölfen, S. Mann, Higher-order organization by mesoscale self-assembly and transformation of hybrid nanostructures, Angew. Chem. Int. Ed. 42 (2003) 2350–2365, https://doi.org/10.1002/anie.200200562.

[5] Y. Ding, Y. Liu, Y. Ren, H. Yan, M. Wang, D. Wang, X.Y. Lu, B. Wang, T. Fan, H. Guo, Controllable synthesis of all the anhydrous CaCO3 polymorphs with various morphologies in CaCl$_2$-NH$_3$-CO$_2$ aqueous system, Powder Technol. 333 (2018) 410–420, https://doi.org/10.1016/j.powtec.2018.04.056.

[6] J. Wang, J. Song, Z. Ji, J. Liu, X. Guo, Y. Zhao, J. Yuan, The preparation of calcium carbonate with different morphologies under the effect of alkanolamide 6502, Colloids Surf. A Physicochem. Eng. Asp. 588 (2020) https://doi.org/10.1016/j.colsurfa.2019.124392.

[7] B. Kanoje, D. Patel, K. Kuperkar, Morphology modification in freshly precipitated calcium carbonate particles using surfactant-polymer template, Mater. Lett. 187 (2017) 44–48, https://doi.org/10.1016/j.matlet.2016.10.043.

[8] M. Kitamura, Crystallization and transformation mechanism of calcium carbonate polymorphs and the effect of magnesium ion, J. Colloid Interface Sci. 236 (2001) 318–327, https://doi.org/10.1006/jcis.2000.7398.

[9] B. Myszka, M. Schüßler, K. Hurle, B. Demmert, R. Detsch, A.R. Boccaccini, S.E. Wolf, Phase-specific bioactivity and altered Ostwald ripening pathways of calcium carbonate polymorphs in simulated body fluid, RSC Adv. 9 (2019) 18232–18244, https://doi.org/10.1039/c9ra01473j.

[10] S. Nam, Y. Park, M.B. Hillyer, R.J. Hron, N. Ernst, S.C. Chang, B.D. Condon, D.J. Hinchliffe, E. Ford, B.C. Gibb, Thermal properties and surface chemistry of cotton varieties mineralized with calcium carbonate polymorphs by cyclic dipping, RSC Adv. 10 (2020) 35214–35225, https://doi.org/10.1039/d0ra06265k.

[11] D. Konopacka-Łyskawa, N. Czaplicka, M. Łapiński, B. Kościelska, R. Bray, Precipitation and transformation of vaterite calcium carbonate in the presence of some organic solvents, Materials (Basel). 13 (2020) 1–14, https://doi.org/10.3390/ma13122742.

[12] M. Ghiasi, M. Abdollahy, M.R. Khalesi, E. Ghiasi, Control of the morphology, specific surface area and agglomeration of precipitated calcium carbonate crystals through a multiphase carbonation process, CrystEngComm. 22 (2020) 1970–1984, https://doi.org/10.1039/c9ce01876j.

[13] S. Polat, Evaluation of the effects of sodium laurate on calcium carbonate precipitation: characterization and optimization studies, J. Cryst. Growth 508 (2019) 8–18, https://doi.org/10.1016/j.jcrysgro.2018.12.017.

[14] Y. Mori, T. Enomae, A. Isogai, Application of vaterite-type calcium carbonate prepared by ultrasound for ink jet paper, J. Imag. Sci. Technol. 54 (2010) 1–6, https://doi.org/10.2352/J.ImagingSci.Technol.2010.54.2.020504.

[15] I. Surya, M. Ginting, The CaCO$_3$-filled natural rubber in the existence of dodecanol: mechanical properties, AIP Conf. Proc. 2197 (2020) 3–9, https://doi.org/10.1063/1.5140927.

[16] F. Pashmforoush, S. Ajori, H.R. Azimi, Interfacial characteristics and thermomechanical properties of calcium carbonate/polystyrene nanocomposite, Mater. Chem. Phys. 247 (2020) 122871, https://doi.org/10.1016/j.matchemphys.2020.122871.

[17] T. Li, Y. Hu, B. Zhang, Biomineralization induced by Colletotrichum acutatum: a potential strategy for cultural relic bioprotection, Front. Microbiol. 9 (2018) 1–8, https://doi.org/10.3389/fmicb.2018.01884.

[18] D. Volodkin, CaCO$_3$ templated micro-beads and -capsules for bioapplications, Adv. Colloid Interf. Sci. 207 (2014) 306–324, https://doi.org/10.1016/j.cis.2014.04.001.

[19] D.B. Trushina, T.V. Bukreeva, M.V. Kovalchuk, M.N. Antipina, CaCO₃ vaterite micro-particles for biomedical and personal care applications, Mater. Sci. Eng. C 45 (2014) 644–658, https://doi.org/10.1016/j.msec.2014.04.050.

[20] M. Kitamura, Controlling factor of polymorphism in crystallization process, J. Cryst. Growth 237–239 (2002) 2205–2214, https://doi.org/10.1016/S0022-0248(01)02277-1.

[21] X. Song, L. Zhang, Y. Cao, J. Zhu, X. Luo, Effect of pH and temperatures on the fast precipitation vaterite particle size and polymorph stability without additives by steamed ammonia liquid waste, Powder Technol. 374 (2020) 263–273, https://doi.org/10.1016/j.powtec.2020.07.029.

[22] L. Ding, B. Wu, P. Luo, Preparation of CaCO₃ nanoparticles in a surface-aerated tank stirred by a long-short blades agitator, Powder Technol. 333 (2018) 339–346, https://doi.org/10.1016/j.powtec.2018.04.057.

[23] F. Liendo, M. Arduino, F.A. Deorsola, S. Bensaid, Optimization of CaCO₃ synthesis through the carbonation route in a packed bed reactor, Powder Technol. 377 (2021) 868–881, https://doi.org/10.1016/j.powtec.2020.09.036.

[24] M. Ukrainczyk, J. Kontrec, V. Babić-Ivančić, L. Brečević, D. Kralj, Experimental design approach to calcium carbonate precipitation in a semicontinuous process, Powder Technol. 171 (2007) 192–199, https://doi.org/10.1016/j.powtec.2006.10.046.

[25] S. Kirboga, M. Öner, Investigating the effect of ultrasonic irradiation on synthesis of calcium carbonate using box-Behnken experimental design, Powder Technol. 308 (2017) 442–450, https://doi.org/10.1016/j.powtec.2016.11.042.

[26] M.A. Popescu, R. Isopescu, C. Matei, G. Fagarasan, V. Plesua, Thermal decomposition of calcium carbonate polymorphs precipitated in the presence of ammonia and alkylamines, Adv. Powder Technol. 25 (2014) 500–507, https://doi.org/10.1016/J.APT.2013.08.003.

[27] N. Czaplicka, D. Konopacka-Łyskawa, Studies on the utilization of post-distillation liquid from Solvay process to carbon dioxide capture and storage, SN Appl. Sci. 1 (2019) https://doi.org/10.1007/s42452-019-0455-y.

[28] Y.S. Han, G. Hadiko, M. Fuji, M. Takahashi, Effect of flow rate and CO₂ content on the phase and morphology of CaCO₃ prepared by bubbling method, J. Cryst. Growth 276 (2005) 541–548, https://doi.org/10.1016/j.jcrysgro.2004.11.408.

[29] Y. Yoo, D. Kang, S. Park, J. Park, Carbon utilization based on post-treatment of desalinated reject brine and effect of structural properties of amines for CaCO₃ polymorphs control, Desalination. 479 (2020) 114325, https://doi.org/10.1016/j.desal.2020.114325.

[30] D. Konopacka-Łyskawa, B. Kościelska, J. Karczewski, A. Gołąbiewska, The influence of ammonia and selected amines on the characteristics of calcium carbonate precipitated from calcium chloride solutions via carbonation, Mater. Chem. Phys. 193 (2017) 13–18, https://doi.org/10.1016/j.matchemphys.2017.01.060.

[31] W. Chuajiw, K. Takatori, T. Igarashi, H. Hara, Y. Fukushima, The influence of aliphatic amines, diamines, and amino acids on the polymorph of calcium carbonate

[32] I. Udrea, C. Capat, E.A. Olaru, R. Isopescu, M. Mihai, C.D. Mateescu, C. Bradu, Vaterite synthesis via gas-liquid route under controlled pH conditions, Ind. Eng. Chem. Res. 51 (2012) 8185–8193, https://doi.org/10.1021/ie202221m.

[33] N. Czaplicka, D. Konopacka-Łyskawa, Utilization of gaseous carbon dioxide and industrial Ca-rich waste for calcium carbonate precipitation: a review, Energies. 13 (2020) 7–14, https://doi.org/10.3390/en13236239.

[34] R. Chang, S. Kim, S. Lee, S. Choi, M. Kim, Y. Park, Calcium carbonate precipitation for CO₂ storage and utilization: a review of the carbonate crystallization and polymorphism, Front. Energy Res. 5 (2017) 1–12, https://doi.org/10.3389/fenrg.2017.00017.

[35] T. Kasikowski, R. Buczkowski, E. Lemanowska, Cleaner production in the ammonia-soda industry: an ecological and economic study, J. Environ. Manag. 73 (2004) 339–356, https://doi.org/10.1016/j.jenvman.2004.08.001.

[36] M. Trypuć, K. Białowicz, CaCO₃ production using liquid waste from Solvay method, J. Clean. Prod. 19 (2011) 751–756, https://doi.org/10.1016/j.jclepro.2010.11.009.

[37] N. Czaplicka, D. Konopacka-Łyskawa, B. Koscielska, M. Łapinski, Effect of selected ammonia escape inhibitors on carbon dioxide capture and utilization via calcium carbonate precipitation, J. CO2 Util. 42 (2020) https://doi.org/10.1016/j.jcou.2020.101298.

[38] C.G. Kontoyannis, N.V. Vagenas, Calcium carbonate phase analysis using XRD and FT-Raman spectroscopy, Analyst. 125 (2000) 251–255, https://doi.org/10.1039/a908609i.

[39] C.Y. Tai, F.B. Chen, Polymorphism of CaCO₃ precipitated in a constant-composition environment, AICHE J. 44 (1998) 1790–1798, https://doi.org/10.1002/aic.690440810.

[40] Y. Sheng Han, G. Hadiko, M. Fuji, M. Takahashi, Crystallization and transformation of vaterite at controlled pH, J. Cryst. Growth 289 (2006) 269–274, https://doi.org/10.1016/j.jcrysgro.2005.11.011.

[41] J. Prah, J. MačEk, G. Dražič, Precipitation of calcium carbonate from a calcium acetate and ammonium carbamate batch system, J. Cryst. Growth 324 (2011) 229–234, https://doi.org/10.1016/j.jcrysgro.2011.03.020.

[42] R.J. Littel, W.P.M. Van Swaaij, G.F. Versteeg, Kinetics of carbon dioxide with tertiary amines in aqueous solution, AICHE J. 36 (1990) 1633–1640, https://doi.org/10.1002/aic.690361103.

[43] G. Puxty, R. Rowland, M. Attalla, Comparison of the rate of CO₂ absorption into aqueous ammonia and monoethanolamine, Chem. Eng. Sci. 65 (2010) 915–922, https://doi.org/10.1016/j.ces.2009.09.042.

precipitated by the introduction of carbon dioxide gas into calcium hydroxide aqueous suspensions, J. Cryst. Growth 386 (2014) 119–127, https://doi.org/10.1016/j.jcrysgro.2013.10.009.